IJRCS

International Journal of Robotics and Control Systems
Vol. 6, No. 1, 2026, pp. 693-717
ISSN 2775-2658
http://pubs2.ascee.org/index.php/ijrcs

ASCEE

Intelligent Chopper and RSC Control Using Crayfish Optimization for Dynamic Stability and Fault Ride-Through of DFIG Wind Turbines

Ahmed Tawfik Hassan [a,1], I. M. Elzein [b,2], Mohamed Metwally Mahmoud [c,d,3,*], Vojtech Blazek [d,4], Alfian Ma'arif [e,5], Ezzeddine Touti [f,6,*], Abdel-Magid M Ali [a,7]

[a] Department of Electrical Engineering, Faculty of Engineering, Aswan University, Aswan 81542, Egypt
[b] Department of Electrical Engineering, College of Engineering and Technology, University of Doha for Science and Technology, Doha P.O. Box 24449, Qatar
[c] Jadara University Research Center, Jadara University, Irbid, Jordan
[d] ENET Centre, CEET, VSB-Technical University of Ostrava, Ostrava, 708 00, Czech Republic
[e] Department of Electrical Engineering, Universitas Ahmad Dahlan, Yogyakarta, Indonesia
[f] Center for Scientific Research and Entrepreneurship, Northern Border University, Arar 73213, Saudi Arabia
[1] EgyptAhmedthhhh@gmail.com; [2] 60101973@udst.edu.qa; [3] metwally_m@aswu.edu.eg; [4] vojtech.blazek@vsb.cz; [5] alfian.maarif@te.uad.ac.id; [6] esseddine.touti@nbu.edu.sa; [7] abdelmagidaly@aswu.edu.eg
* Corresponding Author:

ARTICLE INFO

Article history
Received June 13, 2025
Revised February 26, 2026
Accepted March 12, 2026

Keywords
Doubly Fed Induction Generator;
Fault Ride-Through;
Crayfish Optimization Algorithm;
Dynamic Performance;
Green Energy

ABSTRACT

This paper investigates the enhancement of dynamic performance of a doubly fed induction generator (DFIG)–based wind turbine under variable wind speeds and severe grid fault conditions using a Crayfish Optimization Algorithm (CFO)–based control strategy. The proposed method optimizes the rotor-side converter controller gains and incorporates a braking chopper with CFO-tuned PI controllers to ensure maximum power point tracking and improved fault ride-through capability. The system is evaluated in MATLAB/Simulink under stepwise wind speed variations and an 85% grid voltage dip lasting 150 ms, satisfying grid-code requirements. Simulation results demonstrate fast power coefficient recovery, effective DC-link voltage regulation, reduced current transients, and stable reactive power support. During grid faults, the proposed approach maintains grid connection and enhances post-fault reactive power injection. Comparative results confirm superior transient performance with lower hardware complexity compared to recent optimized DC chopper-based methods.

1. Introduction

WE have proved to be one of the most promising sources of renewable power sources since it produces little environmental impact, is fast advancing in technological innovations and is gradually contributing to the global electricity produced. The DFIG-based WTs have been the most popular among the lot of other technologies in use in wind power systems due to the capacity to work effectively in the fluctuations of wind. Their inherent aspects like variable-speed operation, better P&Q control, and affordability to integrate into the grid are a great improvement in the energy capture, as well as the reliability of the system [1]-[5]. Additionally, the DFIG systems are flexible,

which allows optimal extraction of power as well as rock-steady performance due to sophisticated control mechanisms, such as the use of vector control, adaptive nonlinear controller, and intelligent controllers, including support vector regression and fuzzy-logic-based controllers [3], [6]-[10]. These features can be used to ensure power quality, reduce harmonics, and stabilize the grid, and DFIG-based WTs can therefore be used in large-scale and sustainable wind energy applications [6], [11]-[14].

From the perspective of advantages, DFIGs are still preferred for wind energy conversion systems because P & Q are controlled independently (mainly, through RSC control) [15]-[17]. The independent control capability along with the variable-speed operation allows wind turbines to extract maximum aerodynamic power, while also meeting grid criteria for reactive power and voltage regulation [18], [19]. Consequently, DFIGs demonstrate enhanced dynamic performance, diminished mechanical stress, and lower converter ratings when compared to fully rated converter systems. The implementation of advanced control strategies, such as direct reactive power control, field-oriented control, and intelligent techniques, further mitigates harmonic distortion and power fluctuations, thereby ensuring the injection of high-quality power into the grid [20]-[22].

Notwithstanding these benefits, DFIGs possess an inherent sensitivity to grid disturbances, particularly voltage dips, which can lead to significant over currents in the rotor circuit and over voltages in the DC link. Given that the power electronic converters are only partially rated, their ability to endure these fault-induced transients is limited, rendering FRT capability an essential requirement for contemporary wind turbines [23], [24]. In response to this issue, researchers have devised advanced FRT enhancement techniques, including improved converter topologies, dynamic voltage restorers, fault current limiters, and sophisticated control algorithms such as fuzzy logic and sliding-mode controllers [25]-[29]. The objectives of these solutions include reducing the overcurrent of rotors, controlling the DC-link voltage, and reducing the electromagnetic torque oscillations under grid fault conditions; it also tries to keep the turbine running continuously [30], [31]. Most of the techniques adapt or improve pre-existing converter control strategies, allowing FRT improvement without significant hardware improvements.

Because the transients in DFIG systems caused by faults are severe, protection systems like crowbar circuits and DC choppers are necessary in both preventing faults on the rotor and in sustaining stability during faults by minimizing rotor overcurrent and regulating DC-link voltages [32], [33]. Pertaining to the other variations are rather traditional controllers with fixed or manually adjusted parameters that typically fail to adjust to the changed fault severity or system conditions, risking inefficient energy dissipation, improper rapid response to overvoltage at the DC link, and prolonged transient recovery periods [34]. To overcome these issues, current studies suggest the use of multifunctional DC choppers which can be used both in current-limiting and voltage-limiting modes, without the need to activate the crowbar, thus eliminating rotor-side converter blocking and enhancing transient performance due to severe faults [32]. To ensure that rotor current and DC-link voltage remain within acceptable limits, hybrid hardware-control systems, such as enhanced crowbar activation systems, demagnetizing current controllers, and fault current limiters have also been designed, which improve fault ride-through capability, but tend to add complexity and cost to the system [24]. Moreover, such strategies of implementing intelligent supervisory control, which combine fuzzy logic, genetic algorithm, and IoT-based real-time monitoring, can adjust the parameters of DC-choppers dynamically to have the best performance in cases of grid faults, but a particular optimization of the operation of DC-choppers under extreme fault conditions is also a direction that requires additional research [35], [36]. All in all, the purpose of these advances is to enhance the performance of DFIG fault ride-through by ensuring the balance of the efficacy of protection, complexity of the system and the flexibility of its functioning [32], [35]. The paper presents a more advanced control approach to the DFIG wind systems (Fig. 1) that will enhance the stability of the system and enhance the overall power output.

Although there has been considerable progress in FRT improvement in DFIG systems, there are still various research gaps that have not been addressed. The majority of the literature centers on

converter control enhancement, reactive power compensation, or auxiliary equipment, yet there has not been detailed research on optimized DC-chopper control, which forms a crucial element in eliminating DCL-overvoltage. Mostly based on static or manual tuning, conventional DC-chopper designs possess non-adaptive gains, making them non-adaptive to quickly varying fault conditions, resulting in inadequate protection or, in some cases, development of losses or slower stabilization. Besides, there are not many available studies that explore the application of intelligent optimization algorithms in chopper control, and even those tend to focus on the use of traditional algorithms, including PSO or GSA, which could be slower to converge or less effective in dynamic fault cases [37]. This study is novel since it presents a CFO-based DCL- chopper controller as a first of its kind to improve the FRT capacity of DFIG wind turbines. CFO is well-balanced in exploration and exploitation, converges rapidly, and is resistant to dynamical perturbations, making it very appropriate for real-time tuning of parameters during grid faults. In this work, CFO is applied to adaptively adjust the chopper operation and control parameters to ensure optimal dissipation of excess DC-link energy, effectively limiting overvoltage buildup and reducing rotor overcurrent.

2. DFIG System Description

DFIG is very popular in contemporary WE systems because of VS operation and the ability to offer flexibility in control. It comprises a wound-rotor induction generator connected to the grid by a partially rated power electronic converter that is a combination of an RSC, a GSC and a DC-link capacitor that links the two converters as shown in Fig. 1. A protection crowbar circuit is normally added to provide protection to the converter in the event of faults by temporarily short-circuiting the rotor windings, using resistors. DFIG dynamic behavior is often modeled mathematically as dq-axis, in which the linkages between stator and rotor fluxes, the electromagnetic torque equations and the voltage equations are converted into a synchronous rotating frame to simplify the analysis and control design. Under normal conditions, the RSC modulates the generator torque and reactive power by adjusting the rotor currents to allow efficient extraction of energy over an extensive speed range of wind speed. Meanwhile, the GSC regulates the DC-link voltage and the reactive power support on the grid side ensuring the stable operating conditions and adherence to the requirements of grid codes. This organized control system enables the DFIG to perform with high performance and respond efficiently to grid fluctuations and fluctuating wind speeds.

2.1. Detailed WT Model

This section presents the aerodynamic and mechanical models used to represent the WT driving the DFIG. The model includes (i) the aerodynamic power and torque extracted from the wind, (ii) the tip-speed ratio and power coefficient $C_p(\lambda, \beta)$ representation, (iii) drivetrain dynamics (single- and two-mass options), (iv) gearbox relation, and (v) pitch actuator dynamics. These models are suitable for transient studies such as grid faults, control design (MPPT and pitch control), and interaction with generator converters [38]-[40]. The instantaneous aerodynamic power captured by the rotor is:

$$P_w = \frac{1}{2}\rho A C_p(\lambda, \beta)\, v_w^3 \tag{1}$$

Where ρ is air density (kg/m^3), $A = \pi R^2$ is the rotor swept area (m^2), R is the rotor radius (m), v_w is the wind speed (m/s), β is the pitch angle (deg or rad), and $C_p(\lambda, \beta)$ is the power coefficient. The tip-speed ratio $\lambda$is defined as:

$$\lambda = \frac{\omega_r R}{v_w} \tag{2}$$

where $\omega_r$is the rotor (low-speed shaft) mechanical angular speed (rad/s).

A commonly used parametric representation of $C_p$suitable for control studies is the empirical form:

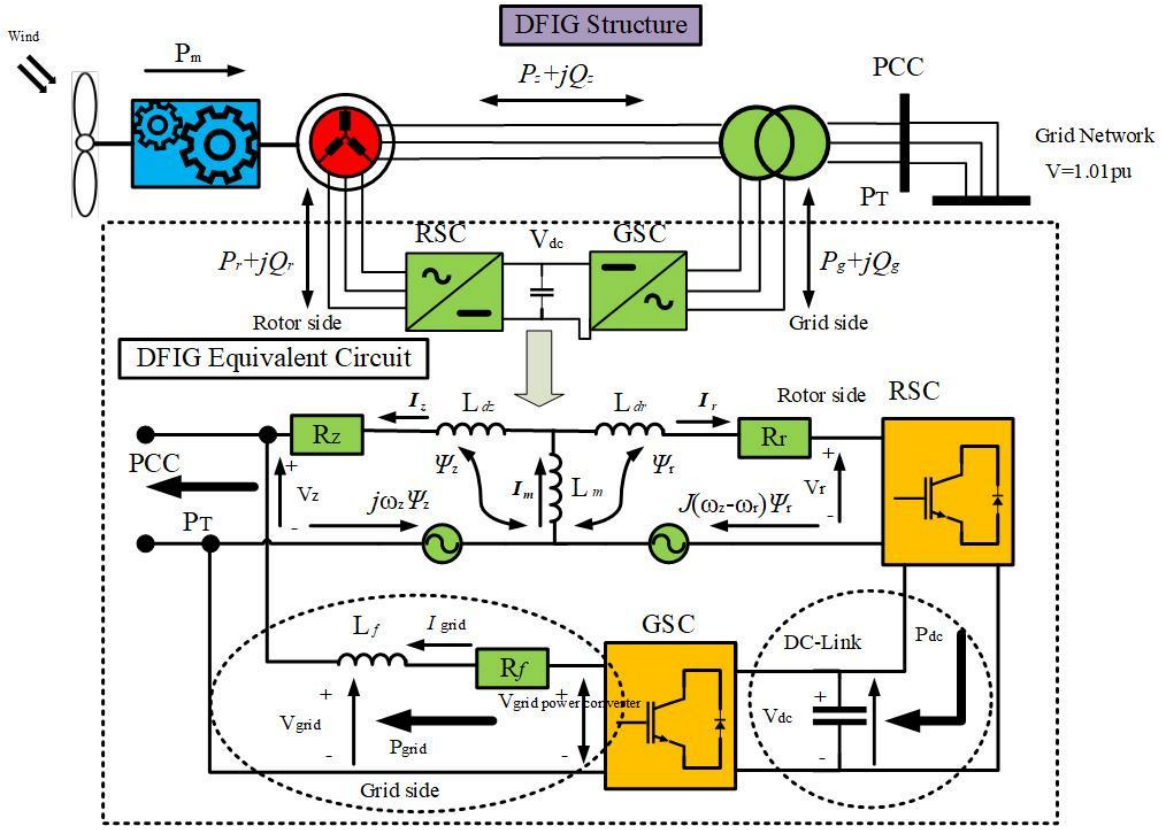

Fig. 1. Detailed description of investigated system

$$C_p(\lambda,\beta) = c_1\left(\frac{c_2}{\lambda_i} - c_3\beta - c_4\beta^{c_5} - c_6\right)e^{-c_7/\lambda_i} \tag{3}$$

With

$$\frac{1}{\lambda_i} = \frac{1}{\lambda + c_8\beta} + c_9(\lambda + c_{10}\beta) \tag{4}$$

where $c_1, \ldots, c_{10}$are curve-fitting constants selected to match the turbine $C_p$curve. For simplified studies you may use a fixed look-up table or polynomial fit $C_p(\lambda,\beta)$derived from manufacturer data. The aerodynamic torque applied to the rotor shaft is:

$$T_a = \frac{P_w}{\omega_r} = \frac{1}{2}\rho A\frac{C_p(\lambda,\beta)\,v_w^3}{\omega_r} \tag{5}$$

When $\omega_r \to 0$(startup) compute torque carefully to avoid division by zero; use the equivalent form $T_a = \frac{1}{2}\rho ARC_p(\lambda,\beta)v_w^2/\lambda$. For many controls and FRT studies a single rigid mass approximation is sufficient:

$$J_t\frac{d\omega_r}{dt} = T_a - T_g - D_t\omega_r \tag{6}$$

where $J_t$is the equivalent inertia of turbine + generator reflected to the rotor side (kg · m^2), $T_g$is the electromagnetic torque supplied by the generator (positive when resisting rotation), and D_t is a viscous damping coefficient.

For more realistic transient torque oscillations use the two-mass model (low-speed rotor side and generator side are separated by shaft stiffness/damping). Denote rotor side by subscript $r$and

generator side by g(generator-side inertia is J_g, angular speed ω_g). Gearbox ratio n (speed-up ratio $n = \omega_g/\omega_r$) is used to reflect generator variables to rotor side:

$$\begin{aligned} J_r \frac{d\omega_r}{dt} &= T_a - K_{sh}\theta_s - D_{sh}\omega_s \\ J_g \frac{d\omega_g}{dt} &= T_g + K_{sh}\theta_s + D_{sh}\omega_s \end{aligned} \tag{7}$$

where the shaft twist angle $\theta_s$and relative speed ω_s are ($\theta_s = \theta_r - \theta_g, \omega_s = \omega_r - \omega_g/n,$) and $K_{sh}$is shaft torsional stiffness (N·m/rad), $D_{sh}$is shaft damping (N·m·s/rad).

For below-rated operation the generator torque reference for MPPT is often computed from the rotor speed setpoint or directly by a power-speed characteristic. A typical MPPT law is:

$$T_g^* = K_{MPPT}\,\omega_r^2 \tag{8}$$

Derived from the optimal tip-speed ratio condition $\lambda^*$and $C_p(\lambda^*)$. Alternatively, a power reference P_{ref}leads to generator torque reference:

$$T_g^* = \frac{P_{ref}}{\omega_g} \tag{9}$$

During FRT scenarios the MPPT loop is overridden by safety controllers that implement current limiting strategies to prevent converter overcurrent and DCL-overvoltage.

2.2. DFIG Mathematical Model

The dynamic behavior of the DFIG can be expressed in the synchronous dq-axis reference frame, where all electrical variables are transformed relative to the grid voltage angle. The stator voltage equations are [41], [42]:

$$v_{ds} = R_s i_{ds} + \frac{d\psi_{ds}}{dt} - \omega_s \psi_{qs} \tag{10}$$

$$v_{qs} = R_s i_{qs} + \frac{d\psi_{qs}}{dt} + \omega_s \psi_{ds} \tag{11}$$

The rotor voltage equations are:

$$v_{dr} = R_r i_{dr} + \frac{d\psi_{dr}}{dt} - (\omega_s - \omega_r)\psi_{qr} \tag{12}$$

$$v_{qr} = R_r i_{qr} + \frac{d\psi_{qr}}{dt} + (\omega_s - \omega_r)\psi_{dr} \tag{13}$$

The dq-axis flux components for the stator and rotor are expressed as:

$$\psi_{ds} = L_s i_{ds} + L_m i_{dr} \tag{14}$$

$$\psi_{qs} = L_s i_{qs} + L_m i_{qr} \tag{15}$$

$$\psi_{dr} = L_r i_{dr} + L_m i_{ds} \tag{16}$$

$$\psi_{qr} = L_r i_{qr} + L_m i_{qs} \tag{17}$$

Where, L_s= stator self-inductance, L_r= rotor self-inductance, L_m= mutual inductance.

The electromagnetic torque equation:

$$T_e = \frac{3}{2}\frac{P}{2}L_m(i_{qs}i_{dr} - i_{ds}i_{qr}) \tag{18}$$

where $P$is the number of poles.

The DFIG mechanical equation:

$$J\frac{d\omega_r}{dt} = T_m - T_e - F\omega_r \tag{19}$$

where J= inertia of the WT + generator, F= friction coefficient, and T_m= mechanical torque from the WT.

The stator P&Q (in dq-frame):

$$\begin{aligned} P_s &= \frac{3}{2}(v_{ds}i_{ds} + v_{qs}i_{qs}), \\ Q_s &= \frac{3}{2}(v_{qs}i_{ds} - v_{ds}i_{qs}). \end{aligned} \tag{20}$$

It used to control torque & Q. The command rotor currents i_{dr} and i_{qr}(in stator-aligned dq frame), so that electromagnetic torque (hence P) and stator Q are regulated. The control mapping (decoupling) is i_{qr} controls torque (P): choose $i_{qr}^*$from a torque/P controller (e.g. MPPT or speed controller). The i_{dr} controls stator Q (or stator flux): choose i_{dr}^* from a Q/voltage controller. Because $T_e \propto (i_{qs}i_{dr} - i_{ds}i_{qr})$, in practice for grid-aligned frame where stator i_{qs}, i_{ds} are known, controllers are tuned so that i_{qr}mainly affects torque and i_{dr}mainly affects Q [43], [44]. Table 1 lists the obtained controllers gains with CFO technique. The proposed RSC control scheme is seen in Fig. 2.

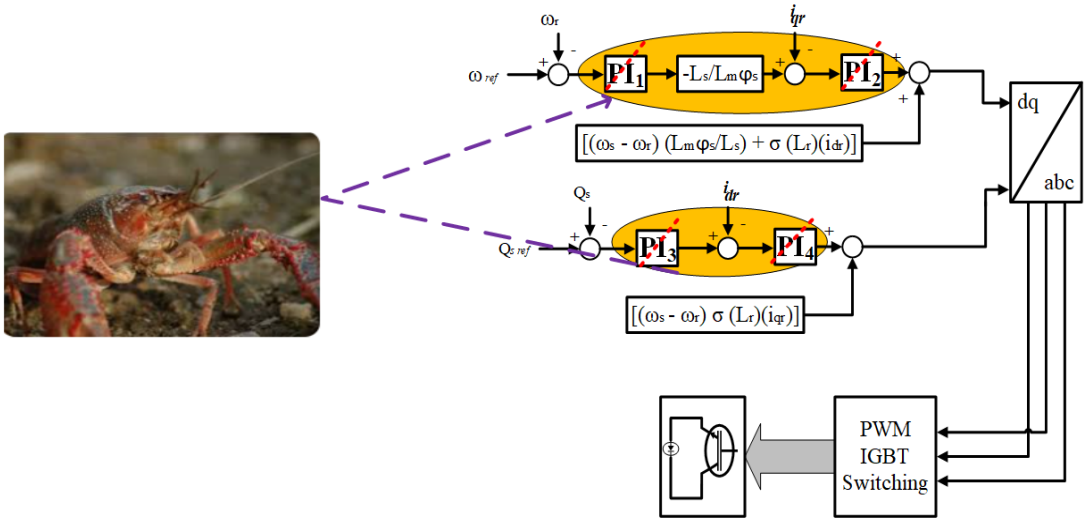

Fig. 2. RSC control scheme

From rotor voltage equations (12) and (13) in dq-frame (stator reference), we implement PI current controllers that compute commanded rotor voltages $v_{dr}^*, v_{qr}^*$to force $i_{dr} \to i_{dr}^*, i_{qr} \to i_{qr}^*$. The PI current controller with decoupling / feedforward are:

$$\begin{aligned} v_{dr}^* &= R_r i_{dr} + \frac{d\psi_{dr}}{dt} - (\omega_s - \omega_r)\psi_{qr} + K_{p,r}(i_{dr}^* - i_{dr}) + K_{i,r}\int (i_{dr}^* - i_{dr})\,dt, \\ v_{qr}^* &= R_r i_{qr} + \frac{d\psi_{qr}}{dt} + (\omega_s - \omega_r)\psi_{dr} + K_{p,r}(i_{qr}^* - i_{qr}) + K_{i,r}\int (i_{qr}^* - i_{qr})\,dt. \end{aligned} \tag{21}$$

Practical implementation replaces $d\psi/dt$ by $L_r\, di_{dr}/dt + L_m\, di_{ds}/dt$ or uses measured decoupling terms; the terms with $(\omega_s - \omega_r)$are the cross-coupling feedforward. The torque (P) setpoint $i_{qr}^*$is produced from a speed/torque controller or power-reference:

$$i_{qr}^* = f_{\text{MPPT/speed}}(\omega_r,\, P_{\text{ref}}). \tag{22}$$

Reactive current setpoint $i_{dr}^*$from a voltage/Q controller:

$$i_{dr}^* = K_Q(Q_{\text{ref}} - Q_s) + i_{dr,\text{bias}}. \tag{23}$$

For FRT, the RSC controller often switches to current-limiting mode where rotor current magnitude $I_r$is limited using:

$$\sqrt{i_{dr}^2 + i_{qr}^2} \le I_{r,max}, \tag{24}$$

Table 1. RSC controllers' gains obtained with CFO method

Controller	PI_1	PI_2	PI_3	PI_4
Gains	K_p = 2.7941 K_i = 0.0848	K_p = 8.0431 K_i = 0.0428	K_p = 0.0893 K_i = 89.174	K_p = 0.3082 K_i = 97.108

2.3. GSC Control System

It controls DCL-voltage & grid Q support. The grid voltage is aligned to the d-axis by a PLL: $v_{dg} = V_g$, $v_{qg} = 0$. Then active and reactive grid powers relate simply to converter currents [45]-[47].

(a) GSC power relations (dq-frame)

$$\begin{aligned} P_g &= \frac{3}{2}\,(v_{dg}i_{dg} + v_{qg}i_{qg}) = \frac{3}{2}\,V_g i_{dg}, \\ Q_g &= \frac{3}{2}\,(v_{qg}i_{dg} - v_{dg}i_{qg}) = -\frac{3}{2}\,V_g i_{qg}. \end{aligned} \tag{25}$$

Thus: i_{dg} controls P to the grid → used to regulate DCL-voltage, and i_{qg}controls Q injection/absorption at the PCC. The energy stored in DC capacitor: $W = \frac{1}{2}CV_{dc}^2$. The time derivative gives:

$$\frac{dW}{dt} = P_{in} - P_{out} - P_{\text{loss}}. \tag{26}$$

Replacing $W$and rearranging:

$$C\,V_{dc}\,\frac{dV_{dc}}{dt} = P_{\text{RSC}} - P_g - P_{\text{loss}}, \tag{27}$$

where P_{RSC} is the power supplied to the DCL from the RSC side (power coming from the rotor/converter pair) and P_g is the P delivered by the GSC to the grid. P_{loss} accounts for converter and filter losses. A PI controller regulates $V_{dc}$and produces the active current reference i_{dg}^*:

$$i_{dg}^* = K_{p,dc}(V_{dc}^{\text{ref}} - V_{dc}) + K_{i,dc}\int (V_{dc}^{\text{ref}} - V_{dc})\, dt. \tag{28}$$

This $i_{dg}^*$is saturated/limited according to the converter rating and then tracked by an inner current loop. The GS-voltage equations (filter + converter) in dq-frame (for the converter terminal currents i_{dg}, i_{qg}):

$$\begin{aligned} v_{dg}^{conv} &= R_f i_{dg} + L_f \frac{di_{dg}}{dt} - \omega_s L_f i_{qg} + v_{dg}^{grid}, \\ v_{qg}^{conv} &= R_f i_{qg} + L_f \frac{di_{qg}}{dt} + \omega_s L_f i_{dg} + v_{qg}^{grid}. \end{aligned} \tag{29}$$

The current controllers compute converter voltage commands v_{dg}^*, v_{qg}^*, often implemented as:

$$\begin{aligned} v_{dg}^* &= R_f i_{dg} + L_f \frac{di_{dg}}{dt} - \omega_s L_f i_{qg} + K_{p,g}(i_{dg}^* - i_{dg}) + K_{i,g}\int (i_{dg}^* - i_{dg})\, dt, \\ v_{qg}^* &= R_f i_{qg} + L_f \frac{di_{qg}}{dt} + \omega_s L_f i_{dg} + K_{p,g}(i_{qg}^* - i_{qg}) + K_{i,g}\int (i_{qg}^* - i_{qg})\, dt. \end{aligned} \tag{30}$$

where the $\pm\omega_s L_f$ terms are the cross-coupling feedforward.

During faults i_{qg}^* is prioritized (subject to converter limits) to inject reactive current for voltage support. To provide grid reactive support during faults, the reactive current reference is obtained from a Q or voltage controller:

$$i_{qg}^* = K_{Qg}(Q_{\text{ref}} - Q_g) \text{ or } i_{qg}^* = K_V(V_{\text{ref}} - V_{PCC}). \tag{31}$$

If the rotor current limit binds, RSC references are scaled and the surplus energy flows to the DC-link; the GSC must then increase i_{dg} to transfer energy to the grid (which helps keep V_{dc} bounded). In practice the control sequence for FRT is: Detect voltage dip → modify i_{dr}^*, i_{qr}^* to avoid overcurrent (current-limiting law or projection). If V_{dc} rises, DC controller increases i_{dg}^* (more active power exported). GSC uses i_{qg} to provide reactive current for voltage support (within converter rating).

A PLL is used to align the control frame with the grid. Outer loops handle torque/MPPT, Q or voltage control, and DCL-regulation, while fast inner current loops use feedforward decoupling. During FRT, current limiting and DC-chopper action (or CFO-optimized control) manage converter saturation and balance i_d–i_q priorities. The GSC controllers gains has been listed in [42]. The implemented GSC control scheme is seen in Fig. 3.

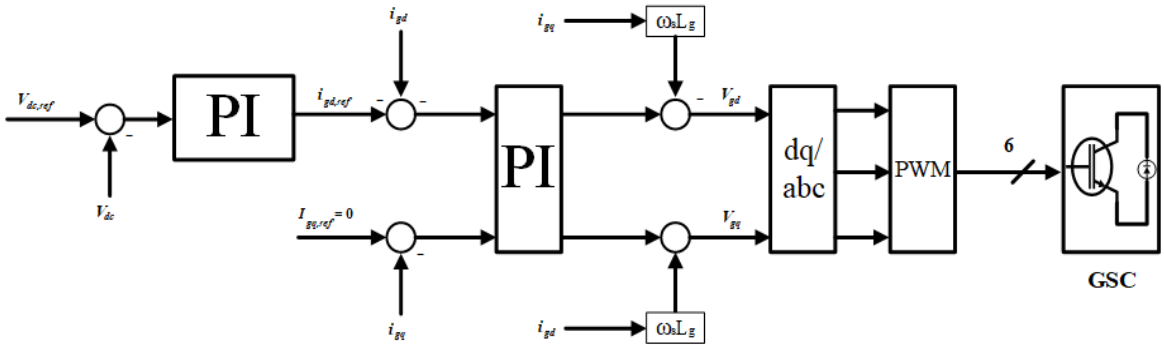

Fig. 3. GSC control scheme

3. FRT Problem in DFIG-Based WTs

Voltage dips in DFIG systems pose significant risks because they generate large transient rotor currents that can exceed converter limits and trigger protection mechanisms [48]. These high currents lead to RSC overloading, risking converter shutdown and loss of control. At the same time, voltage dips raise the DC-link voltage, stressing the capacitor and power electronics and potentially activating crowbar or chopper protection [49]. The sudden electromagnetic torque variations introduced by these disturbances also generate torque oscillations, increasing mechanical stress on the shaft and drivetrain and shortening equipment lifespan [50]. In case the converters lose contact

with overcurrent or excessive voltage, the DFIG is deprived of P&Q control, causing the system to become unstable and causing turbines to lose contact [51]. This issue is even worse in asymmetrical dips where negative-sequence components form extra torque fluctuations and DC-link ripples which further jeopardize the stability of the system [52], [53].

Considering such difficulties, effective defense during grid faults is a precondition to guarantee the stability of DFIG and avoid the destruction of converters. Conventional approaches like crowbar circuits and DC choppers reduce overcurrent and overvoltage however they tend to bring about disadvantages such as converter blocking or poor energy dissipation [48]. To address these shortcomings, more recent studies have aimed at multifunctional DC choppers that can operate both in current-limiting and voltage-limiting modes without necessarily requiring crowbar activation so that transient behavior is smoother and FRT performance is enhanced [49]. Further optimization methods, such as multi-objective particle swarm optimization, and fuzzy-based tuning, further optimize the settings of a chopper and improve the collaboration of reactive current injection to prevent oscillations caused by faults [50]. Also, hybrid techniques that incorporate modified crowbars, fault current limiters and improved control algorithms provide superior voltage control and current limiting, but at the cost of increased complexity and hardware demands [51]. All these enhancements are intended to ensure that the DFIG fault response becomes stronger but does not adversely affect the operational flexibility in different grid conditions [52], [53]. Fig. 4 presents an overview of DFIG FRT techniques [54].

Such protection and control improvements are particularly essential since the current grid codes demand DFIG-based WTs to maintain connectivity during voltage dips of up to 15% for durations between 150 and 625 ms to ensure grid stability during disturbances [55]. Under these circumstances, the WTs must contribute reactive current to assist in voltage recovery, as highlighted in Spain, Germany, and Denmark, among other countries (Fig. 5) [56], [54]. To meet these standards, higher levels of FRT control measures should coordinate the activities of RSC and GSC to control overcurrent, limit the increase in DC-link voltage, and ensure the required level of reactive power injection [54]. The GC curves represent the minimum voltage profile to which turbines must remain connected, reflecting increasingly stringent global requirements [28], [55]. Other methods, such as minimum threshold crowbar activation and voltage disturbance compensation, can further expand the stable operation range of DFIGs, especially in weak grids [56]. Therefore, greater FRT compliance ensures that wind turbines remain connected to the grid in the event of faults, preventing significant power losses and enhancing overall system reliability [57].

4. Control Strategy to Achieve FRT Capability

4.1. Crowbar Protection

DFIG systems short-circuit the rotor using resistors to ensure the safety of the RSC in the event of a grid fault, which causes the DFIG to act like a squirrel-cage induction generator and makes them less controllable with high Q consumption [32]. The crowbar limits rotor overcurrent by bypassing the rotor converter, but it blocks the RSC, preventing the DFIG from fully complying with grid codes that require Q injection during faults [58]. To address DC-link overvoltage, a DC-link chopper dissipates excess energy by switching a resistor across the DC-link capacitor, preventing voltage spikes and protecting the converter [33]. Coordinated control of crowbar and DC-link chopper protections improves FRT capability by limiting rotor current and DC-link voltage simultaneously, allowing better transient performance and grid support. Recent advances propose multifunctional DC choppers that can operate without crowbar activation, maintaining converter control and enhancing FRT without the drawbacks of crowbar blocking [32]. Overall, combining crowbar and DC-link chopper protections, or replacing crowbars with advanced DC chopper schemes, balances converter protection with grid code compliance and improved DFIG controllability during faults [59]. The FRT strategy managing P and Q in inverter driven DFIG has been described in Fig. 6 [60]. The dynamic behavior of the crowbar during fault conditions can be represented using a simplified mathematical

model. When activated, the crowbar introduces a protection resistor, and the resulting voltage across the branch is given by:

$$V_C = F_S R_C I_C \tag{32}$$

where $F_S$denotes the switching status of the crowbar device.

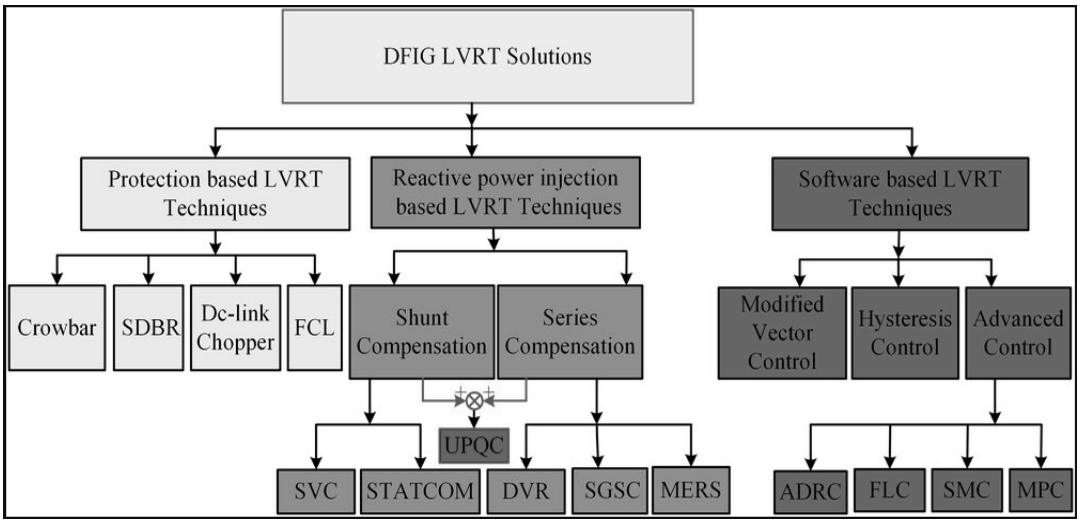

Fig. 4. Summary of DFIG FRT methods [54]

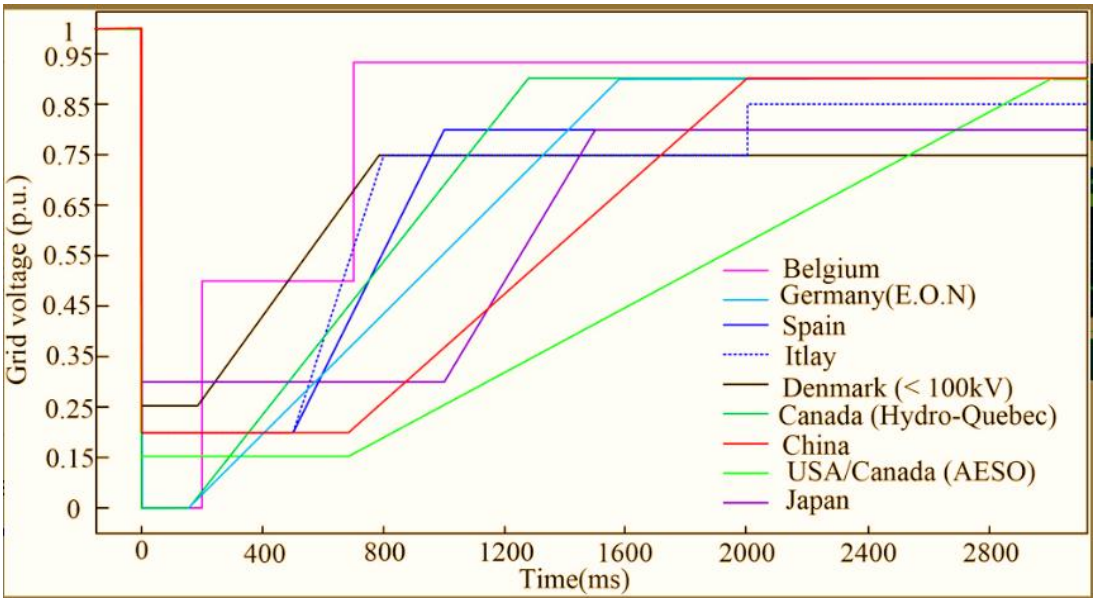

Fig. 5. FRT requirements set by leading WE-countries [54]

The equivalent rotor short-circuit time constant is expressed as:

$$T_r^{SC} = \frac{L_r^{SC}}{R_r + R_{\tau c}} \tag{33}$$

Characterizing the transient response of the rotor during crowbar conduction. The maximum rotor current can be approximated by:

$$I_r^{\max} = \frac{V_r^{\max}}{\sqrt{(X_r^{SC})^2 + (R_{\tau c})^2}} \tag{34}$$

Ensuring the rotor current remains within safe limits under fault conditions. To avoid excessive current peaks, the crowbar resistance must satisfy:

$$R_{\tau c} < \frac{\sqrt{2}\, X_{rs}^{SC} V_r^{\max}}{\sqrt{3.2 V_s^2 + 2(V_r^{\max})^2}} \tag{35}$$

Providing a criterion for proper sizing of the protection element. The rotor voltage during this interval can be related to the DC-link voltage through:

$$V_r = k\, m\, V_{DC}, k = \frac{1}{\sqrt{3}} \frac{V_{DC}^b}{V_r^b} \tag{36}$$

Highlighting the influence of modulation and base quantities on rotor voltage levels. The maximum rotor voltage typically satisfies:

$$V_r^{\max} = IR_{DC} - V_{DC} = 0 \tag{37}$$

These conditions define the border in designing crowbar protection. These equations determine the electrical behaviors of the crowbar circuit and will be used effectively to integrate the crowbar circuit into the DFIG fault protection strategies.

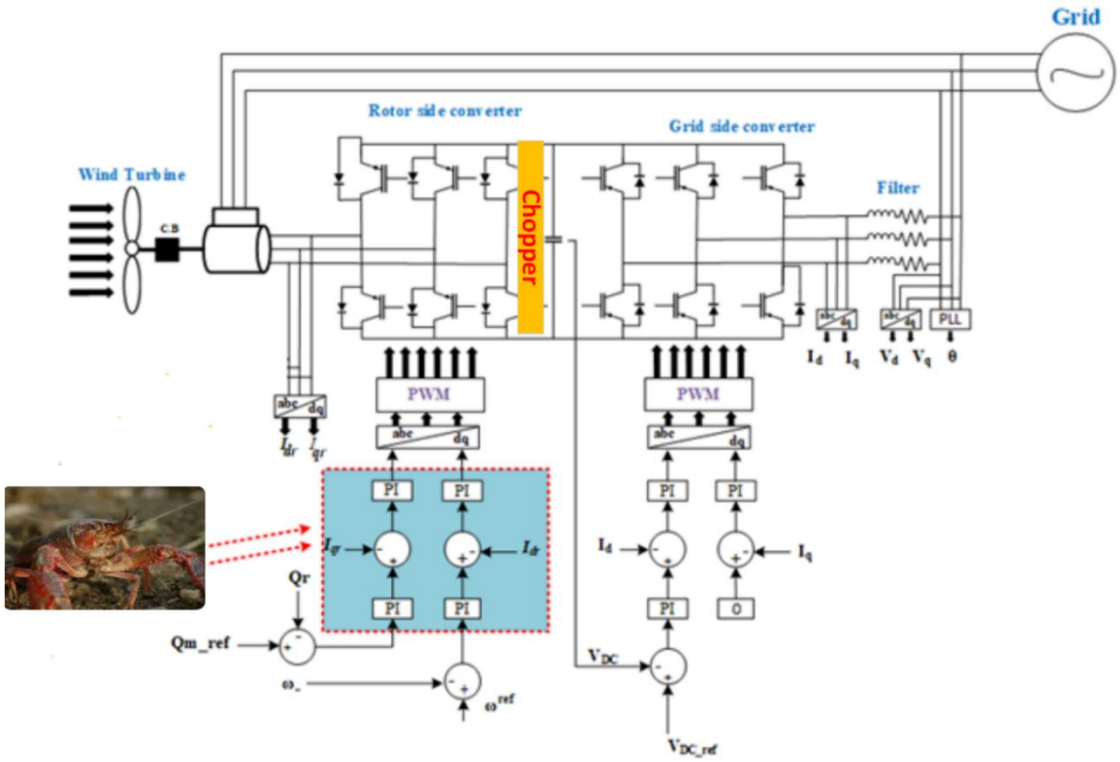

Fig. 6. FRT strategy managing P and Q in inverter-driven DFIG

4.2. CFO Technique

The CFO algorithm mimics crayfish behaviors, seeking cooler areas, competing, and foraging, represented through three phases that balance exploration and exploitation. A random initial population begins the search, and a temperature-based rule determines whether the algorithm explores new regions or refines existing solutions. In the foraging phase, each candidate moves toward the best solution, using a simplified mechanism inspired by crayfish breaking large food items to improve feeding efficiency. This adaptive structure enables CFO to transition smoothly between global search and local optimization for faster convergence [61], [62].

(A) CFO initialization phase

The controller parameters operate within predefined bounds, and CFO begins by generating an initial population within these limits using Eq. (32) [63], [64]:

$$X_{i,j} = \text{rand} \times (UB_j - LB_j) + LB_j \tag{38}$$

All solutions form the matrix shown in Eq. (38):

$$X = \begin{bmatrix} X_{1,1} & X_{1,j} & \cdots & X_{1,\text{dim}} \\ X_{i,1} & X_{i,j} & \cdots & X_{i,\text{dim}} \\ \vdots & \vdots & \ddots & \vdots \\ X_{N,1} & X_{N,j} & \cdots & X_{N,\text{dim}} \end{bmatrix} \tag{39}$$

Each solution is evaluated via a fitness function, and the values are stored in:

$$f_{\text{fitness}} = [f1f2f3 \ldots \ldots \ldots \ldots f_N]^T \tag{40}$$

(B) Temperature and feeding behavior

Crayfish actions depend on the temperature computed in Eq. (35) [63]:

$$Temp = \text{rand} \times 15 + 20 \tag{41}$$

Feeding efficiency follows a Gaussian relation (Eq. (36)):

$$p = C_1 \left(\frac{1}{\sqrt{2\pi}\sigma} e^{-(Temp-\mu)^2/(2\sigma^2)} \right) \tag{42}$$

(C) Exploration: summer resort

When $Temp > 30°\text{C}$, crayfish move to cooler regions. The shaded target is [63]:

$$X_{\text{shade}} = (X_G + X_L)/2 \tag{43}$$

If rand < 0.5, an individual updates its position using Eq. (38):

$$X_{i,j}^{t+1} = X_{i,j}^t + C_2 \times \text{rand} \times (X_{\text{shade}} - X_{i,j}^t) \tag{44}$$

with the coefficient:

$$C_2 = 2 - (t/T) \tag{45}$$

(D) Exploitation: competition

If rand ≥ 0.5under high temperature, multiple individuals target the same cave, resulting in competition [63]:

$$X_{i,j}^{t+1} = X_{i,j}^t - X_{z,j}^t + X_{\text{shade}} \tag{46}$$

where the competing individual is chosen by:

$$z = \text{round}(\text{rand} \times (N-1) + 1) \tag{47}$$

(E) Exploitation: foraging

When $Temp \leq 30°\text{C}$, crayfish move toward the global best [63]:

$$X_{\text{food}} = X_G \tag{48}$$

The food-size factor is:

$$Q = C_3 \times \text{rand} \times (fitness_i / fitness_{\text{food}}) \tag{49}$$

If the food is large:

$$X_{\text{food}} = e^{-1/Q} \times X_{\text{food}} \tag{50}$$

The resulting movement is:

$$X_{i,j}^{t+1} = X_{i,j}^{t} + X_{\text{food}} \times p(\cos(2\pi \text{ rand}) - \sin(2\pi \text{ rand})) \tag{51}$$

Otherwise:

$$X_{i,j}^{t+1} = (X_{i,j}^{t} - X_{\text{food}}) \times p + p \times \text{rand} \times X_{i,j}^{t} \tag{52}$$

These mechanisms collectively allow CFO to adjust its exploration and exploitation behavior dynamically. A complete flow of the algorithm is shown in Fig. 7.

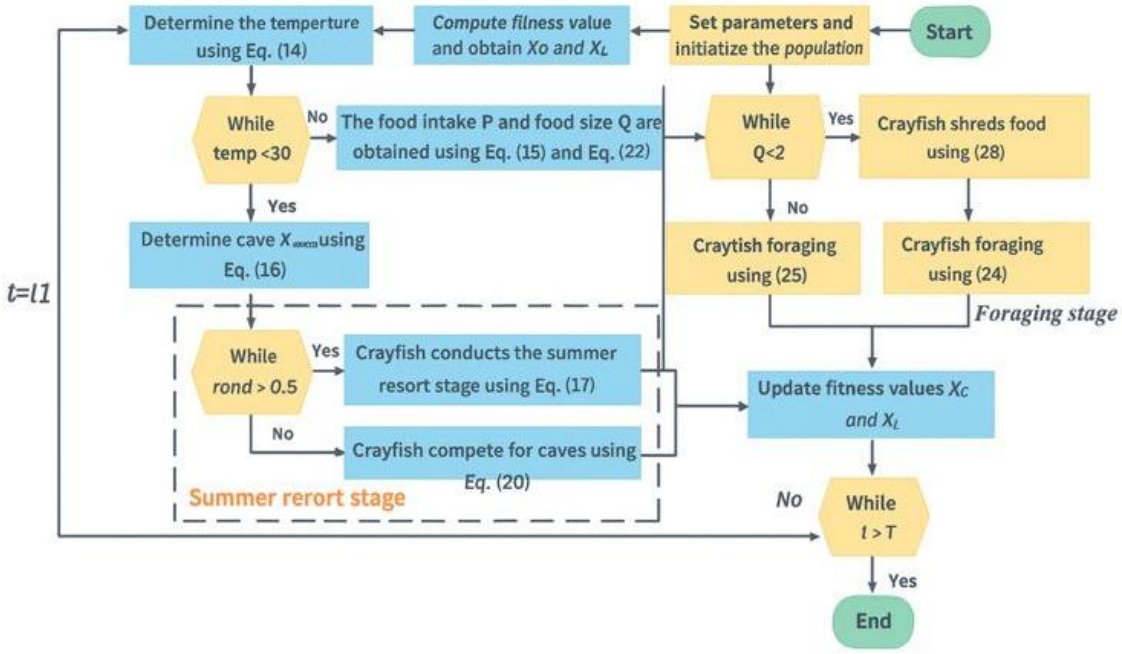

Fig. 7. Flowchart of CFO [61]

4.3. Applications of CFO-Based PI Controller

This work employs the CFO algorithm to tune the PI controller responsible for enhancing the DFIG performance. CFO begins with randomly generated PI gains and evaluates each set using the ITAE fitness metric. Candidate solutions are iteratively updated by learning from the best performers until the stopping condition is met. The optimized $K_p$and $K_i$values are then applied to achieve stable and accurate DCL voltage control. The optimization objective is given by:

$$OF = \int_0^T t \mid (V_{dc}^{ref} - V_{dc}^{act}) + (P^{ref} - P^{act}) + (Q^{ref} - Q^{act}) + (T^{ref} - T^{act}) \mid dt \tag{53}$$

Grid faults can cause overspeed, torque oscillations, excessive currents, and DC link overvoltage in DFWG systems. Since the converters are highly sensitive, effective FRT and protection schemes are essential. The crowbar circuit offers reliable protection during these events, allowing the generator to stay connected and maintain energy delivery. The optimized PI gains ($K_p = K_i = 0.06553$) govern the switching signals that activate the chopper. The proposed chopper-based DFWG control scheme is presented in Fig. 8.

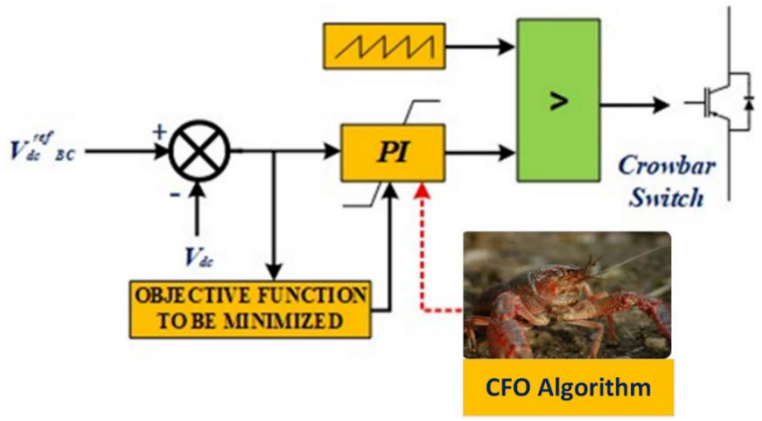

Fig. 8. Proposed control system of crowbar based on CFO-PI controller

5. Results and Discussions

This study examines the enhancement of DFIG dynamic behavior under varying wind conditions and grid disturbances to highlight the effectiveness of the CFO. A severe voltage sag of 0.15 p.u. is investigated when DFIG equipped with the proposed crowbar-based CFO control scheme. The system response is evaluated using key performance indicators, including active power (P), DCL voltage, and Q, to assess the influence of the proposed control strategy on overall machine performance. The investigated DFIG-based WT system is modeled and simulated in MATLAB/Simulink to validate the proposed approach in enhancing the dynamic performance under changeable wind speed and achieving FRT capability. The detailed system parameters are provided in [65].

5.1. Effects of Fluctuations in Wind Speed within Standard Grid Parameters

The wind speed varies in discrete steps over the 50 s simulation period, starting at approximately 12 m/s, dropping to about 8 m/s at 10 s, then rising again to nearly 12 m/s around 15 s, before increasing further to about 15 m/s and finally decreasing to approximately 12 m/s at 35 s, where it remains until the end of the simulation (Fig. 9 (a)). These step changes impose varying aerodynamic loads and evaluate the WT's dynamic response. Correspondingly, the power coefficient C_p closely follows the wind variations, increasing from 0.2 to 0.48 during higher wind speeds, dropping to around 0.32 after wind reduction, and stabilizing near 0.20 when the wind decreases again at 35 s, reflecting effective aerodynamic adaptation (Fig. 9 (b)). The pitch angle initially starts near 9° and rapidly decreases to 0° to maximize power capture at moderate wind speeds, remaining near zero until about 20 s. When wind speed increases significantly at 25 s, the pitch controller raises the blade angle to approximately 8–9.9° to limit power and rotor torque, before returning smoothly to 0° after 35 s, indicating effective pitch regulation (Fig. 9 (c)). The P&Q are shown in Fig. 9 (d), where Q is maintained at zero due to unity power factor operation, while active power follows wind variations. The nearly constant DCL voltage in Fig. 9 (e) confirms efficient power transfer to the grid. The very small oscillations observed in all variables demonstrate the effectiveness of the proposed PAC strategy combined with the CFO-PI controller under changing wind conditions. Table 2 lists a numerical comparison between the proposed method and previously published works to show the role of the proposed technique.

5.2. Impact of Severe Fault

The DFIG performance with the proposed optimized controllers is assessed under an 85% voltage dip lasting 150 ms, representing a worst-case grid-code condition (Fig. 10 (a)). During the fault, active power drops while rotor and stator current, reactive power, and DCL-voltage increase (Fig. 10 (b)-(e)). The braking chopper limits the DCL voltage by dissipating excess energy, and post-fault reactive power injection is maintained while the DFIG remains grid-connected, confirming effective FRT under severe disturbances.

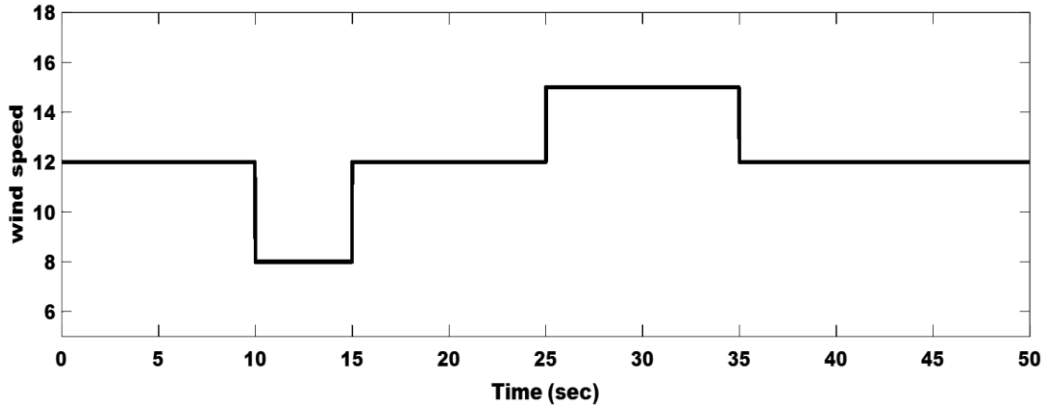

(a) wind speed profile

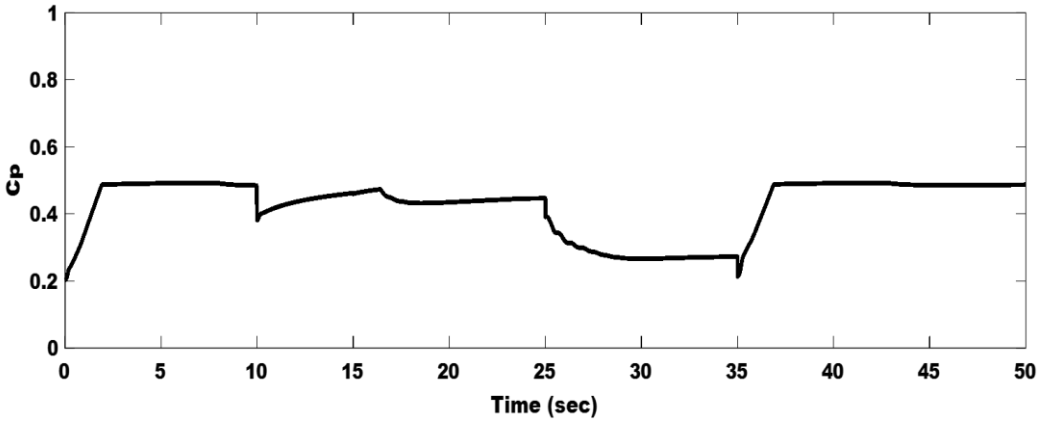

(b) Power coefficient

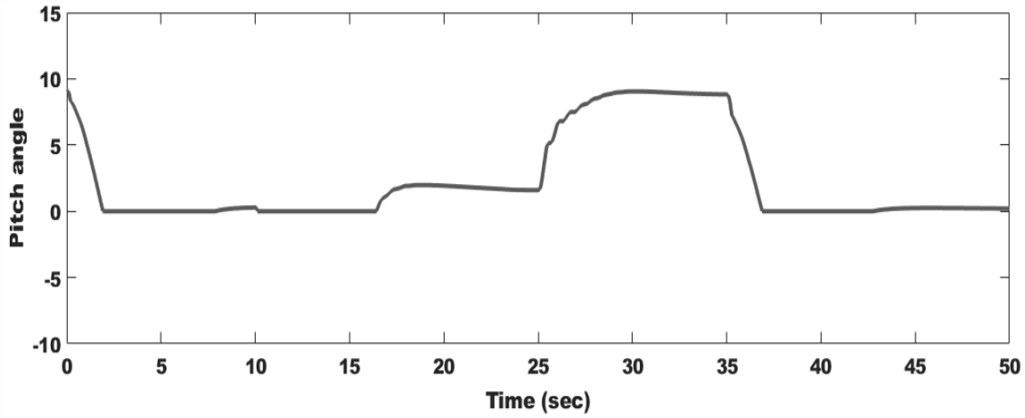

(c) Pitch angle

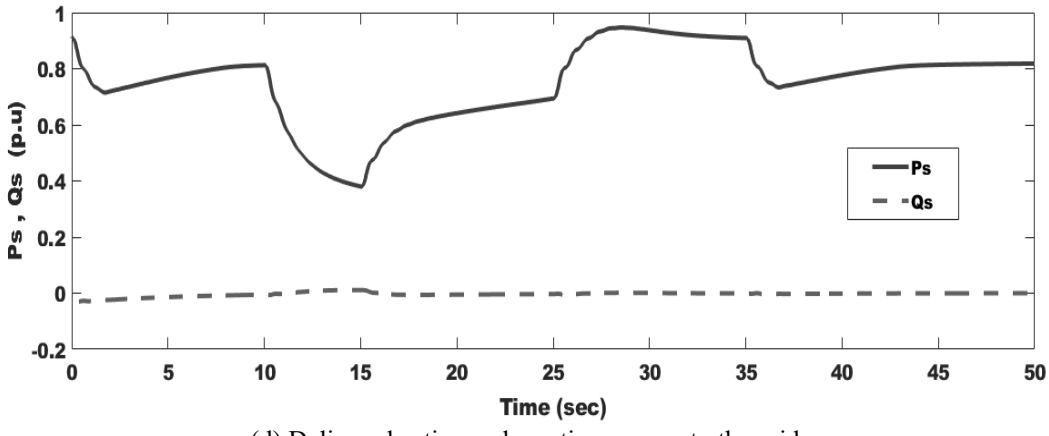

(d) Delivered active and reactive powers to the grid

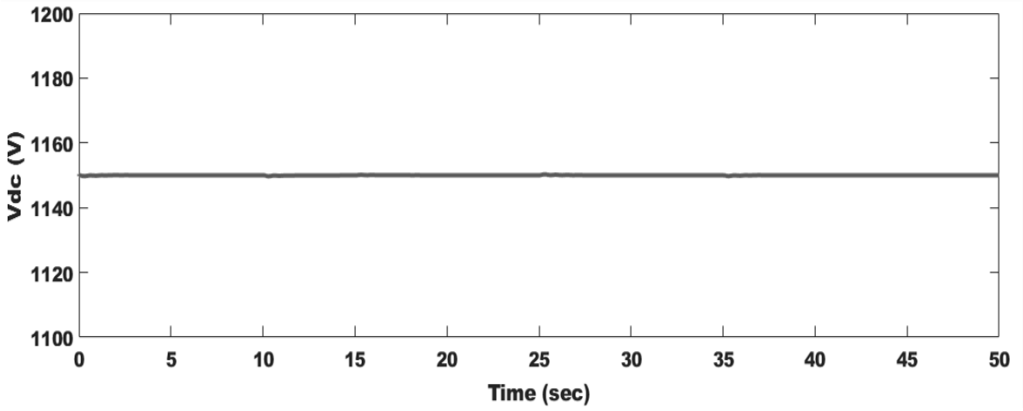

(e) DCL voltage

Fig. 9. DFIG's system parameters response as a result of wind speed changes

Table 2. Numerical comparison between the proposed method and previously published works

Performance Metric	Conventional PI / MPPT [66], [67]	PSO / GA-based control [68], [69]	FRT-focused DFIG control [70], [71]	Proposed CFO-PI method
Maximum (C_p)	0.44 – 0.46	0.46 – 0.47	0.45 – 0.46	**≈ 0.48**
C_p recovery after wind step	Slow, oscillatory	Moderate oscillations	Moderate	**Fast, smooth recovery**
Maximum pitch angle (°)	12 – 15°	10 – 14°	10 – 13°	**≤ 9.9°**
DCL voltage overshoot	25 – 40% (1.3–1.5 p.u.)	15 – 20%	20 – 30%	**< 10%**
DCL voltage ripple	High	Medium	Medium	**Very low**
Q deviation (p.u.)	±0.2 – ±0.4	±0.15 – ±0.3	±0.2 – ±0.35	**≈ 0 (unity PF)**
Rotor speed variation (pu)	±0.05 – ±0.08	±0.04 – ±0.06	±0.04 – ±0.07	**±0.01 – ±0.02**
Mechanical stress mitigation	Limited	Moderate	Moderate	**High**
GC compliance	Partial	Improved	Improved	**Fully compliant**

Several recent studies have focused on improving the FRT capability of DFIG-based WTs through optimized chopper control strategies. Ref. [32] proposed a multifunctional DC chopper with nonlinear control that operates without a crowbar, successfully limiting DC-link voltage and rotor current during severe faults. While effective, their approach relies on nonlinear control complexity and continuous converter operation. In contrast, the present work combines an optimized chopper controller with optimized RSC controllers, ensuring robust protection of the RSC under an 85% voltage dip lasting 150 ms, while still maintaining grid connection and reactive power injection. Refs., [72], [73] employed superconducting coils coordinated with DC choppers optimized using Elephant Herding Optimization, Harmony Search, and Grey Wolf Optimization. These solutions achieved strong DC-link voltage regulation and current suppression; however, they introduce high cost, cryogenic requirements, and increased system complexity. The proposed method in this paper attains comparable DC-link voltage limitation using conventional hardware, making it more practical for large-scale deployment. Ref. [36] applied multi-objective particle swarm optimization (MOPSO) to coordinate braking chopper control and reactive current injection, improving transient performance and damping mechanical oscillations. Similarly, the proposed scheme enhances transient stability, but it further demonstrates continuous grid connection and controlled Q injection during and after the fault, satisfying stringent grid-code requirements. Ref. [70] developed a PSO-optimized nonlinear DC chopper controller for offshore wind farms, achieving improved DCL-voltage stabilization compared to classical controllers. The present study extends this concept by integrating an active crowbar, ensuring both electrical and converter protection under deep voltage dips.

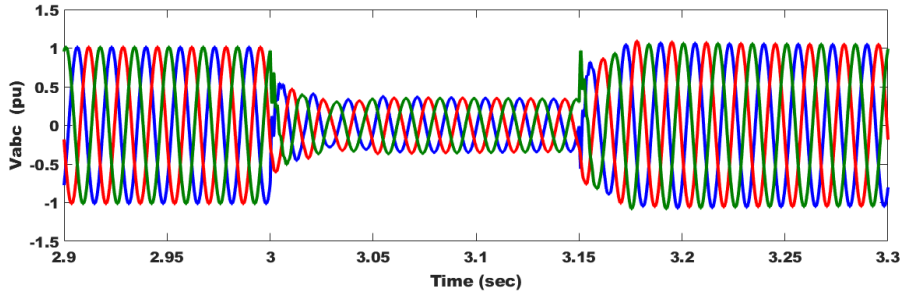

(a)

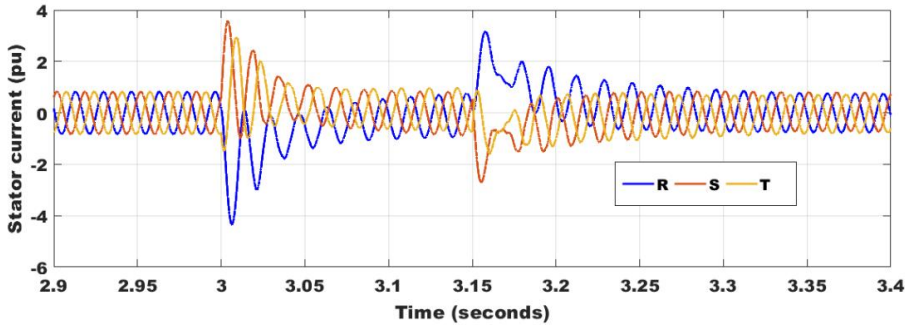

(b)

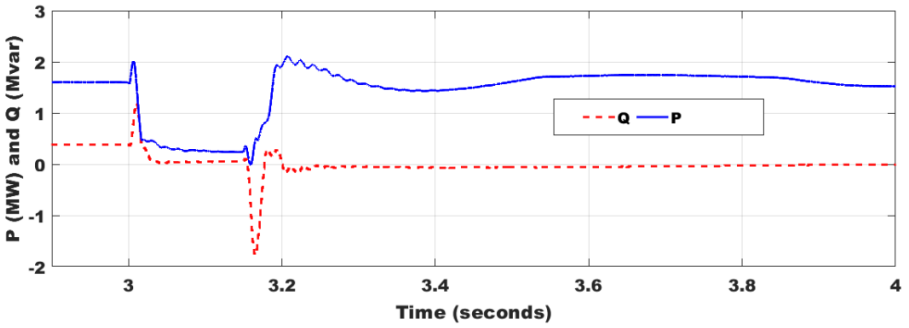

(c)

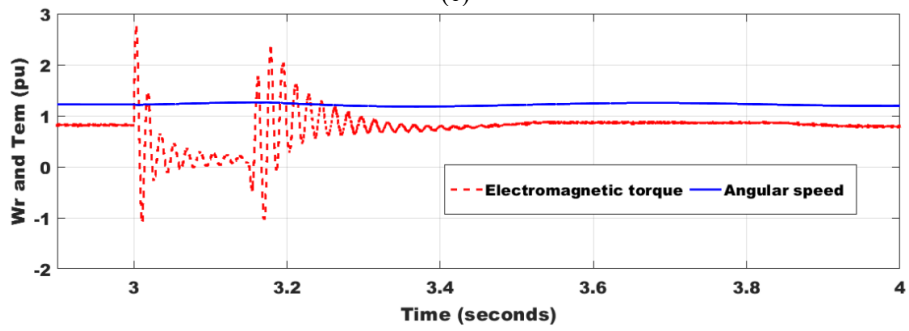

(d)

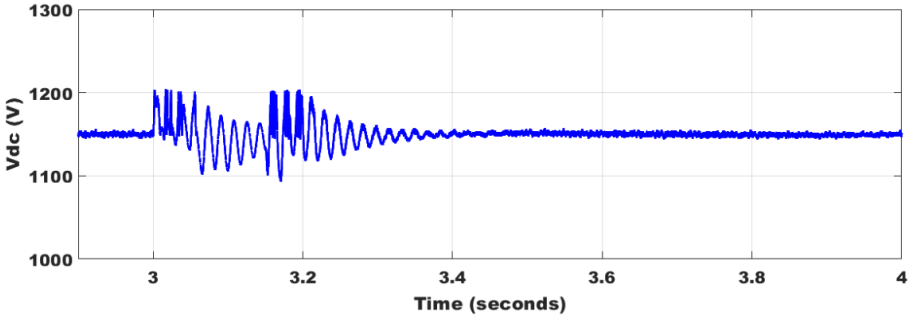

(e)

Fig. 10. DFWG's system parameters response as a result of 85% VD

Ref. [74] proposed a modified DC chopper topology with additional semiconductor switches to insert series/parallel resistances, allowing fault current limitation without blocking the RSC. Although effective, the added hardware increases system complexity. By comparison, the proposed approach achieves similar FRT performance through control coordination rather than hardware expansion, offering a simpler and cost-effective solution. Overall, this work distinguishes itself by achieving strong FRT performance under worst-case grid conditions using a coordinated active crowbar and optimized control strategy, balancing protection effectiveness, GC compliance, and implementation simplicity. Numerical and qualitative comparison with existing works is presented in Table 3.

Table 3. Numerical and qualitative comparison with existing works

Ref.	Protection strategy	Optimization method	Fault severity	DCL voltage control	Q support	Hardware complexity
[32]	Multifunctional DC chopper (no crowbar)	Nonlinear control	Severe VDs	Strong limitation	Yes	Medium
[73]	DC chopper + superconducting coil	HS + GWO	Voltage faults	Excellent	Yes	Very high
[72]	DC chopper + superconducting coil	EHO-PI	Ferro resonance overvoltage	Excellent	Limited	Very high
[36]	Braking chopper + Q injection	MOPSO	Grid faults	Good	Strong	Medium
[70]	Nonlinear DC chopper	PSO	Offshore grid faults	Good	Moderate	Medium
[74]	Modified DC chopper topology	Rule-based	Voltage dips	Good	Limited	High
This work	Active crowbar + optimized controllers	CFO-PI / optimized control	85% VD, 150 ms	It kept within safe limits (~1.04 pu)	Yes (post-fault Q injection)	Low–Medium

5.3. PQ Assessment

The close agreement among phases suggests that the control strategy effectively mitigates harmonics without introducing phase asymmetry, contributing to stable and reliable grid-connected operation.) with the literature: THD in DFIG systems is generally maintained at low levels to ensure PQ and grid code compliance. Ref. [75] demonstrated that under various conditions, including unbalanced nonlinear loads and varying wind speeds, the stator currents of DFIG maintain low THD within IEEE 519 standards. Ref. [76] showed that using a robust model predictive control with self-filtering can reduce rotor current THD drastically, achieving reductions over 99% compared to before filtering. Ref. [77] designed a proportional resonance controller with harmonic compensators that mitigates sub-synchronous resonance without compromising THD in power signals. Ref. [78] found that optimizing the DC link capacitor value minimizes stator and rotor current THD across different speeds. Ref. [79] applied a chaotic Salp swarm optimization-tuned neuro-fuzzy controller that reduced grid current THD below 2.85%, improving voltage stability and harmonic suppression. Ref. [80] compared sinusoidal PWM and third harmonic injection PWM techniques in diode-clamped multilevel inverters, achieving THD below 5% across wind speeds. Ref. [81] proposed an improved extended power theory method that reduces stator current THD and torque oscillations under voltage unbalance. Ref. [82] reported THD values around 1.46% to 2.03% under different operating modes using an advanced backstepping controller 11. These studies collectively highlight that advanced control methods and hardware optimization effectively reduce THD in DFIG systems, enhancing power quality and grid compliance.

Fig. 11 illustrates the THD obtained from the system under variable wind speed, where the proposed control strategy achieves measured THD levels of 0.16%, 0.17%, and 0.15% in the R, S,

and T phases, respectively. These values are significantly below the maximum thresholds specified by IEEE and IEC standards, confirming excellent PQ performance and demonstrating strong harmonic suppression due to the controller's filtering and adaptive capabilities. When benchmarked against IEEE 519 standard limits, the approach achieves an overall harmonic reduction between 94% and 98%, highlighting its effectiveness in mitigating distortion and ensuring reliable grid-connected operation. Under severe voltage dip conditions, the harmonic distortion levels remain nearly identical across all three phases, with an extremely small spread of 0.02% (Fig. 12), indicating excellent phase balance and uniform harmonic behavior. All THD values stay below the IEEE 519 recommended limit of 5%, confirming acceptable PQ and compliance with grid standards.

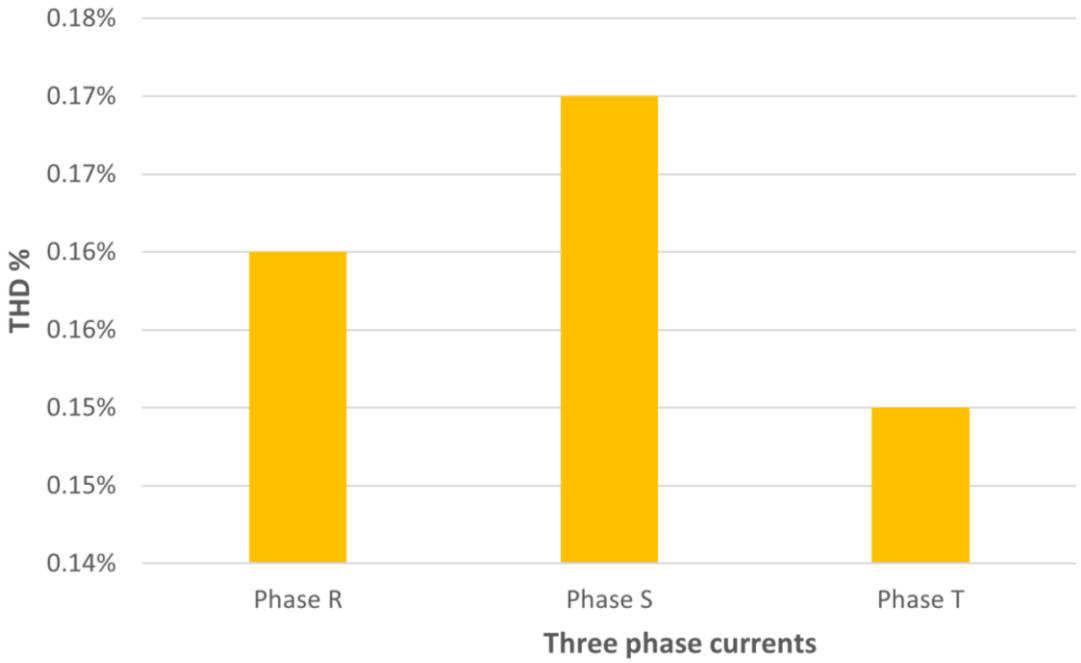

Fig. 11. % THD under variable wind speed

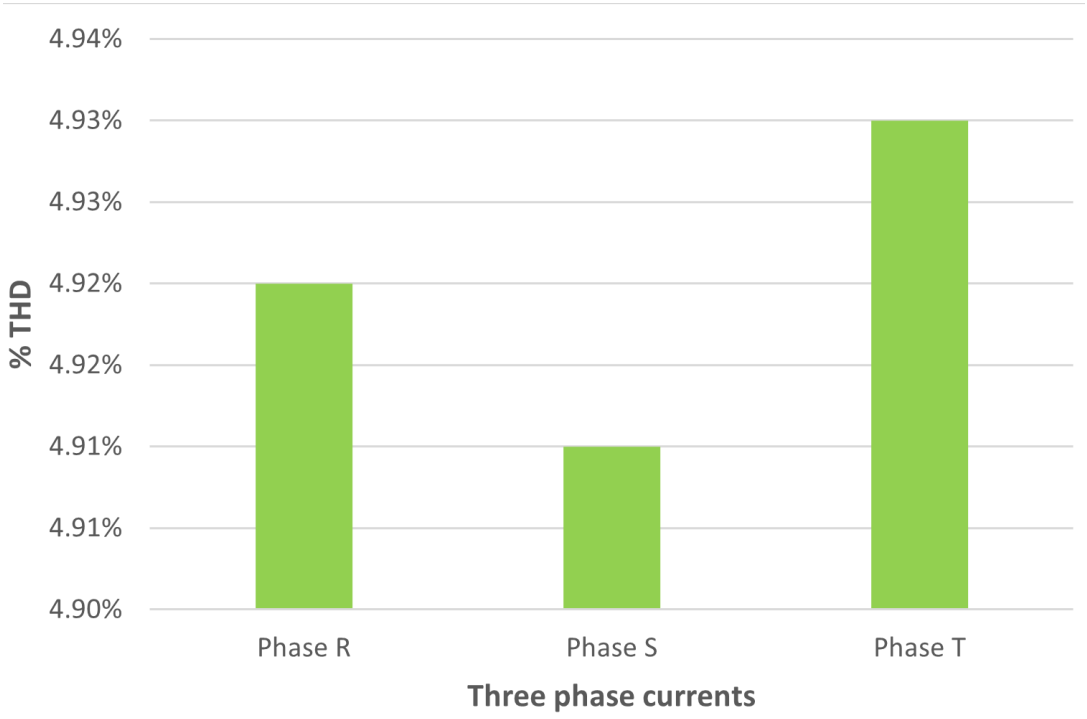

Fig. 12. %THD under voltage dip

6. Conclusion

This paper presents a CFO-based chopper control strategy to enhance the dynamic performance and FRT of DFIG-based WTs. It achieves a maximum Cp of almost 0.48 under variable wind speed conditions, which is higher compared to the 0.44-0.47 range of conventional PI- and PSO-based controllers. The system also demonstrates fast and smooth recovery from wind speed variations. The pitch angle is limited to a maximum of about 9.9°, reducing mechanical stress compared to earlier reports of 10-15°. The DCL- voltage overshoot is kept below 10%, a significant improvement over the 25-40% seen in conventional methods. The Q deviation remains almost zero for unity power factor operation, ensuring compliance with grid codes. Validation of the proposed strategy was conducted under severe grid fault conditions, including an 85% VD lasting for 150 ms, representing a real-life worst-case scenario. Simulation results show that the DCL-voltage was clamped at approximately 1.04 p.u., preventing overvoltage in the converter and damping currents spikes. Post-fault clearance, active power was smoothly restored, and Q injection was maintained without disconnecting from the grid. The presented approach demonstrates similar or better performance compared to recent optimized DC chopper-based solutions, which report DCL- voltage excursions of 1.15-1.3 p.u. potentially requiring additional hardware and increasing complexity. Overall, these results confirm that the CFO-based control strategy is effective and robust in providing reliability and resilience for DFIG-based wind energy systems under normal and faulted conditions.

Data Availability: The data used to support the findings of this study are available at reasonable request from the corresponding author.

Conflicts of Interest: The authors declare that they have no conflicts of interest.

Acknowledgment: The authors extend their appreciation to the Deanship of Scientific Research at Northern Border University, Arar, KSA for funding this research work through the project number "NBU-FFR-2026-2448-05". Also, this article has been produced with the financial support of the European Union under the REFRESH-Research Excellence for REgion Sustainability and High-tech Industries project number CZ.10.03.01/00/22_003/0000048 via the Operational Programme Just Transition.

References

[1] A. A. B. M. Zin, M. H. A. Pesaran, A. B. Khairuddin, L. Jahanshaloo, and O. Shariati, "An overview on doubly fed induction generators′ controls and contributions to wind based electricity generation," *Renewable and Sustainable Energy Reviews*, vol. 27. pp. 692-708, 2013, https://doi.org/10.1016/j.rser.2013.07.010.

[2] F. Echiheb *et al*., "Experimental evaluation of an advanced predictive control technique for variable-speed wind turbine systems," *International Journal of Electrical Power & Energy Systems*, vol. 168, p. 110668, 2025, https://doi.org/10.1016/j.ijepes.2025.110668.

[3] M. G. Kebede and M. B. Tuka, "Power Control of Wind Energy Conversion System with Doubly Fed Induction Generator," *Journal of Energy*, vol. 2022, no. 1, pp. 1–12, 2022, https://doi.org/10.1155/2022/8679053.

[4] O. M. Lamine *et al*., "A Combination of INC and Fuzzy Logic-Based Variable Step Size for Enhancing MPPT of PV Systems," *International Journal of Robotics and Control Systems*, vol. 4, no. 2, pp. 877-892, 2024, https://doi.org/10.31763/ijrcs.v4i2.1428.

[5] F. Menzri, T. Boutabba, I. Benlaloui, H. Bawayan, M. I. Mosaad, and M. M. Mahmoud, "Applications of hybrid SMC and FLC for augmentation of MPPT method in a wind-PV-battery configuration," *Wind Engineering*, vol. 48, no. 6, pp. 1186-1202, 2024, https://doi.org/10.1177/0309524X241254364.

[6] F. Nasim, S. Khatoon, I. Nasiruddin, M. Shahid, S. Urooj, and B. Bilal, "Support-Vector-Regression-Based Intelligent Control Strategy for DFIG Wind Turbine Systems," *Machines*, vol. 13, no. 8, p. 687, 2025, https://doi.org/10.3390/machines13080687.

[7] S. Ouhssain *et al*., "Performance Optimization of a DFIG-based Variable Speed Wind Turbines by IVC-ANFIS Controller," *Journal of Robotics and Control*, vol. 5, no. 5, pp. 1492-1501, 2024, https://doi.org/10.18196/jrc.v5i5.22118.

[8] N. Benalia *et al*., "Enhancing electric vehicle charging performance through series-series topology resonance-coupled wireless power transfer," *PLOS One*, vol. 19, no. 8, p. e0309545, 2024, https://doi.org/10.1371/journal.pone.0309545.

[9] M. M. Hussein, T. H. Mohamed, M. M. Mahmoud, M. Aljohania, M. I. Mosaad, and A. M. Hassan, "Regulation of multi-area power system load frequency in presence of V2G scheme," *PLOS One*, vol. 18, no. 9, p. e0291463, 2023, https://doi.org/10.1371/journal.pone.0291463.

[10] A. T. Hassan *et al*., "Adaptive Load Frequency Control in Microgrids Considering PV Sources and EVs Impacts: Applications of Hybrid Sine Cosine Optimizer and Balloon Effect Identifier Algorithms," *International Journal of Robotics and Control Systems*, vol. 4, no. 2, pp. 941–957, 2024, https://doi.org/10.31763/ijrcs.v4i2.1448.

[11] A. Mishra, P. M. Tripathi, and K. Chatterjee, "A review of harmonic elimination techniques in grid connected doubly fed induction generator based wind energy system," *Renewable and Sustainable Energy Reviews*, vol. 89. pp. 1-15, 2018, https://doi.org/10.1016/j.rser.2018.02.039.

[12] B. S. Atia *et al*., "Applications of Kepler Algorithm-Based Controller for DC Chopper: Towards Stabilizing Wind Driven PMSGs under Nonstandard Voltages," *Sustainability*, vol. 16, no. 7, p. 2952, 2024, https://doi.org/10.3390/su16072952.

[13] O. M. Kamel, I. M. Elzein, M. M. Mahmoud, A. Y. Abdelaziz, M. M. Hussein, and A. A. Z. Diab, "Effective energy management strategy with a novel design of fuzzy logic and JAYA-based controllers in isolated DC/AC microgrids: A comparative analysis," *Wind Engineering*, vol. 49, no. 1, pp. 199-222, 2025, https://doi.org/10.1177/0309524X241263518.

[14] H. Alnami, S. A. E. M. Ardjoun, and M. M. Mahmoud, "Design, implementation, and experimental validation of a new low-cost sensorless wind turbine emulator: Applications for small-scale turbines," *Wind Engineering*, vol. 48, no. 4, pp. 565–579, 2024, https://doi.org/10.1177/0309524X231225776.

[15] S. Tamalouzt *et al*., "Enhanced direct reactive power control-based multi-level inverter for dfig wind system under variable speeds," *Sustainability*, vol. 13, no. 16, p. 9060, 2021, https://doi.org/10.3390/su13169060.

[16] V. S. K. Lagudu, D. V. N. Ananth, and S. Madichetty, "Independent control of active and reactive power for grid connected DFIG using reference power based improved field-oriented control scheme," *International Journal of Ambient Energy*, vol. 43, no. 1, pp. 3252–3265, 2022, https://doi.org/10.1080/01430750.2020.1818123.

[17] F. Menzri *et al*., "Applications of Novel Combined Controllers for Optimizing Grid-Connected Hybrid Renewable Energy Systems," *Sustainability*, vol. 16, no. 16, p. 6825, 2024, https://doi.org/10.3390/su16166825.

[18] H. Benbouhenni, I. Colak, N. Bizon, M. I. Mosaad, and T. G. Tella, "Power regulation of variable speed multi rotor wind systems using fuzzy cascaded control," *Scientific Reports*, vol. 14, no. 1, p. 16415, 2024, https://doi.org/10.1038/s41598-024-67194-4.

[19] A. P. Padamata and G. S. Rao, "Modelling of Variable Speed Wind Turbine Connected DFIG:250KW," *WSEAS Transactions on Power Systems*, vol. 18, pp. 426-435, 2023, https://doi.org/10.37394/232016.2023.18.42.

[20] T. Douadi, Y. Harbouche, R. Abdessemed, I. Bakhti, "Improvement Performances of Active and Reactive Power Control Applied to DFIG for Variable Speed Wind Turbine Using Sliding Mode Control and FOC," *International Journal of Engineering*, vol. 31, no. 10, pp. 1689-1697, 2018, https://www.ije.ir/article_82209.html.

[21] M. A. Alarabi and S. Sünter, "ANN-Based Maximum Power Tracking for a Grid-Synchronized Wind Turbine-Driven Doubly Fed Induction Generator Fed by Matrix Converter," *Energies*, vol. 18, no. 10, p. 2521, 2025, https://doi.org/10.3390/en18102521.

[22] S. Basu *et al*., "Applications of Snow Ablation Optimizer for Sustainable Dynamic Dispatch of Power and Natural Gas Assimilating Multiple Clean Energy Sources," *Engineering Reports*, vol. 7, no. 6, pp. 1-12, 2025, https://doi.org/10.1002/eng2.70211.

[23] N. Jabbour, E. Tsioumas, C. Mademlis and E. Solomin, "A Highly Effective Fault-Ride-Through Strategy for a Wind Energy Conversion System With a Doubly Fed Induction Generator," *IEEE Transactions on Power Electronics*, vol. 35, no. 8, pp. 8154-8164, 2020, https://doi.org/10.1109/TPEL.2020.2967971.

[24] S. Saeed, R. Asghar, F. Mehmood, H. Saleem, B. Azeem, and Z. Ullah, "Evaluating a Hybrid Circuit Topology for Fault-Ride through in DFIG-Based Wind Turbines," *Sensors*, vol. 22, no. 23, p. 9314, 2022, https://doi.org/10.3390/s22239314.

[25] R. A. J. Amalorpavaraj, P. Kaliannan, S. Padmanaban, U. Subramaniam and V. K. Ramachandaramurthy, "Improved Fault Ride Through Capability in DFIG Based Wind Turbines Using Dynamic Voltage Restorer With Combined Feed-Forward and Feed-Back Control," *IEEE Access*, vol. 5, pp. 20494-20503, 2017, https://doi.org/10.1109/ACCESS.2017.2750738.

[26] L. Xian, L. Wu, W. Li, Y. Wu, and X. Xie, "Enhancing FRT capability of DFIG based on RC-crowbar considering the resonance and matching control strategies for different fault degrees," *Electric Power Systems Research*, vol. 232, p. 110434, 2024, https://doi.org/10.1016/j.epsr.2024.110434.

[27] P. M. Tripathi, A. Mishra, and K. Chatterjee, "Fault ride through/low voltage ride through capability of doubly fed induction generator–based wind energy conversion system: a comprehensive review," *Modeling and Control Dynamics in Microgrid Systems with Renewable Energy Resources*, pp. 275-311, 2023, https://doi.org/10.1016/B978-0-323-90989-1.00008-7.

[28] G. A. Parameswari and H. H. Sait, "A comprehensive review of fault ride-through capability of wind turbines with grid-connected doubly fed induction generator," *International Transactions on Electrical Energy Systems*, vol. 30, no. 8, 2020, https://doi.org/10.1002/2050-7038.12395.

[29] M. T. Mohamed *et al*., "Sustainable Energy Management in Islanded Microgrids via HHO-BE Tuned Adaptive Controllers and Demand-Side Flexibility," *Engineering Reports*, vol. 8, no. 1, pp. 1-20, 2026, https://doi.org/10.1002/eng2.70561.

[30] A. M. S. Yunus, A. Abu-Siada, M. A. S. Masoum, M. F. El-Naggar and J. X. Jin, "Enhancement of DFIG LVRT Capability During Extreme Short-Wind Gust Events Using SMES Technology," *IEEE Access*, vol. 8, pp. 47264-47271, 2020, https://doi.org/10.1109/ACCESS.2020.2978909.

[31] S. R. Mosayyebi, S. H. Shahalami, and H. Mojallali, "Fault ride-through capability improvement in a DFIG-based wind turbine using modified ADRC," *Protection and Control of Modern Power Systems*, vol. 7, no. 1, p. 50, 2022, https://doi.org/10.1186/s41601-022-00272-9.

[32] C. Yan, W. Wang, Z. Liu, H. Yang, H. Liu and B. Zhang, "A Simple Multifunctional DC Chopper for Fault Ride-Through Capacity Enhancement of a DFIG," *IEEE Transactions on Power Electronics*, vol. 40, no. 9, pp. 12048-12054, 2025, https://doi.org/10.1109/TPEL.2025.3565530.

[33] M. Liu *et al*., "An Electromagnetic Transient Analysis Model for DFIG Considering LVRT Hardware Protection," *IEEE Access*, vol. 9, pp. 32591-32598, 2021, https://doi.org/10.1109/ACCESS.2021.3060409.

[34] A. K. Singh, D. K. Tiwari, N. B. D. Choudhury, and J. Singh, "A grid-compliant control approach for current reference generation strategy to improve Low-Voltage Ride-Through (LVRT) performance and power management in grid-tied PV system," *Computers and Electrical Engineering*, vol. 128, p. 110638, 2025, https://doi.org/10.1016/j.compeleceng.2025.110638.

[35] C. R. Raghavendran, J. Preetha Roselyn, and D. Devaraj, "Development and performance analysis of intelligent fault ride through control scheme in the dynamic behaviour of grid connected DFIG based wind systems," *Energy Reports*, vol. 6, pp. 2560-2576, 2020, https://doi.org/10.1016/j.egyr.2020.07.015.

[36] M. E. B. Aguilar, D. V. Coury, R. Reginatto, R. M. Monaro, P. T. de Godoy, and T. G. Jahn, "Multi-Objective PSO for Control-Loop Tuning of DFIG Wind Turbines with Chopper Protection and Reactive-Current Injection," *Energies*, vol. 17, no. 1, p. 28, 2024, https://doi.org/10.3390/en17010028.

[37] A. F. A. Ahmed, I. M. Elzein, M. M. Mahmoud, S. A. E. M. Ardjoun, A. M. Ewias, and U. Khaled, "Optimal Controller Design of Crowbar System for DFIG-based WT: Applications of Gravitational

Search Algorithm," *Buletin Ilmiah Sarjana Teknik Elektro*, vol. 7, no. 2, pp. 122-137, 2025, https://doi.org/10.12928/biste.v7i2.13027.

[38] M. M. Mahmoud, "Improved current control loops in wind side converter with the support of wild horse optimizer for enhancing the dynamic performance of PMSG-based wind generation system," *International Journal of Modeling and Simulation*, vol. 43, no. 6, pp. 952-966, 2023, https://doi.org/10.1080/02286203.2022.2139128.

[39] M. M. Mahmoud *et al*., "Application of Whale Optimization Algorithm Based FOPI Controllers for STATCOM and UPQC to Mitigate Harmonics and Voltage Instability in Modern Distribution Power Grids," *Axioms*, vol. 12, no. 5, p. 420, 2023, https://doi.org/10.3390/axioms12050420.

[40] M. M. Mahmoud *et al*., "Evaluation and Comparison of Different Methods for Improving Fault Ride-Through Capability in Grid-Tied Permanent Magnet Synchronous Wind Generators," *International Transactions on Electrical Energy Systems*, vol. 2023, 2023, https://doi.org/10.1155/2023/7717070.

[41] I. E. Maysse *et al*., "Nonlinear Observer-Based Controller Design for VSC-Based HVDC Transmission Systems Under Uncertainties," *IEEE Access*, vol. 11, pp. 124014-124030, 2023, https://doi.org/10.1109/ACCESS.2023.3330440.

[42] M. M. Mahmoud, B. S. Atia, A. Y. Abdelaziz, and N. A. N. Aldin, "Dynamic Performance Assessment of PMSG and DFIG-Based WECS with the Support of Manta Ray Foraging Optimizer Considering MPPT, Pitch Control, and FRT Capability Issues," *Processes*, vol. 10, no. 12, p. 2723, 2022, https://doi.org/10.3390/pr10122723.

[43] H. Boudjemai *et al*., "Application of a Novel Synergetic Control for Optimal Power Extraction of a Small-Scale Wind Generation System with Variable Loads and Wind Speeds," *Symmetry*, vol. 15, no. 2, p. 369, 2023, https://doi.org/10.3390/sym15020369.

[44] M. M. Mahmoud *et al*., "Integration of Wind Systems with SVC and STATCOM during Various Events to Achieve FRT Capability and Voltage Stability: Towards the Reliability of Modern Power Systems," *International Journal of Energy Research*, vol. 2023, 2023, https://doi.org/10.1155/2023/8738460.

[45] M. M. Mahmoud, M. M. Aly, H. S. Salama, and A. M. M. Abdel-Rahim, "Dynamic evaluation of optimization techniques-based proportional–integral controller for wind-driven permanent magnet synchronous generator," *Wind Engineering*, vol. 45, no. 3, pp. 696-709, 2021, https://doi.org/10.1177/0309524X20930421.

[46] M. M. Mahmoud, H. S. Salama, M. M. Aly, and A. M. M. Abdel-Rahim, "Design and implementation of FLC system for fault ride-through capability enhancement in PMSG-wind systems," *Wind Engineering*, vol. 45, no. 5, pp. 1361-1373, 2021, https://doi.org/10.1177/0309524X20981773.

[47] M. M. Mahmoud, M. K. Ratib, M. M. Aly, and A. M. M. Abdel–Rahim, "Application of Whale Optimization Technique for Evaluating the Performance of Wind-Driven PMSG Under Harsh Operating Events," *Process Integration and Optimization for Sustainability*, vol. 6, no. 2, pp. 447-470, 2022, https://doi.org/10.1007/s41660-022-00224-8.

[48] Y. Yang, M. Gao, and Z. Zhou, "Enhanced Control Strategies for Improving Low Fault Ride-Through Capability of Grid-Connected Doubly Fed Induction Wind Turbines," *Energies*, vol. 18, no. 4, p. 767, 2025, https://doi.org/10.3390/en18040767.

[49] A. Loulijat, N. Ababssi, and M. Mohamed, "Kalman Observer Contribution to a Second Order Sliding Mode Control for Wind Turbine Based on DFIG During the Network Voltage Dip," *International Journal of Intelligent Engineering and Systems*, vol. 14, no. 5, pp. 88-101, 2021, https://doi.org/10.22266/ijies2021.1031.09.

[50] R. A. de Oliveira, C. Chen, M. H. J. Bollen and R. Chouhy Leborgne, "Comparative Analysis of Transformer-Energizing and Fault-Caused Voltage Dips on the Dynamic Behavior of DFIG-Based Wind Turbines," *2020 IEEE PES Innovative Smart Grid Technologies Europe (ISGT-Europe)*, pp. 589-593, 2020, https://doi.org/10.1109/ISGT-Europe47291.2020.9248983.

[51] M. B. Tuka, "Investigation of Voltage Dip Problems during Faults on a Grid-Tied Doubly Fed Induction Generator in a Wind Energy System," *Jordan Journal of Electrical Engineering*, vol. 9, no. 2, pp. 209-227, 2023, https://doi.org/10.5455/jjee.204-1669028936.

[52] Y. Zhou, P. Bauer, J. A. Ferreira and J. Pierik, "Operation of Grid-Connected DFIG Under Unbalanced Grid Voltage Condition," *IEEE Transactions on Energy Conversion*, vol. 24, no. 1, pp. 240-246, 2009, https://doi.org/10.1109/TEC.2008.2011833.

[53] A. M. Nori, A. K. Abdulabbas, and T. M. Aljohani, "Coordinated Sliding Mode and Model Predictive Control for Enhanced Fault Ride-Through in DFIG Wind Turbines," *Energies*, vol. 18, no. 15, p. 4017, 2025, https://doi.org/10.3390/en18154017.

[54] Z. Din, J. Zhang, Z. Xu, Y. Zhang, and J. Zhao, "Low voltage and high voltage ride-through technologies for doubly fed induction generator system: Comprehensive review and future trends," *IET Renewable Power Generation*, vol. 15, no. 3, pp. 614-630, 2021, https://doi.org/10.1049/rpg2.12047.

[55] A. H. K. Alaboudy, H. A. Mahmoud, A. A. Elbaset, and M. Abdelsattar, "Technical Assessment of the Key LVRT Techniques for Grid-Connected DFIG Wind Turbines," *Arabian Journal for Science and Engineering*, vol. 48, no. 11, pp. 15223-15239, 2023, https://doi.org/10.1007/s13369-023-07975-7.

[56] Z. Li, H. Xu, Z. Wang and Q. Yan, "Stability Assessment and Enhanced Control of DFIG-Based WTs During Weak AC Grid," *IEEE Access*, vol. 10, pp. 41371-41380, 2022, https://doi.org/10.1109/ACCESS.2022.3166810.

[57] W. K. Ntuli, M. Kabeya, and K. Moloi, "Review of Low Voltage Ride-Through Capabilities in Wind Energy Conversion System," *Energies*, vol. 17, no. 21, p. 5321, 2024, https://doi.org/10.3390/en17215321.

[58] A. M. A. Haidar, K. M. Muttaqi and M. T. Hagh, "A Coordinated Control Approach for DC link and Rotor Crowbars to Improve Fault Ride-Through of DFIG-Based Wind Turbine," *IEEE Transactions on Industry Applications*, vol. 53, no. 4, pp. 4073-4086, 2017, https://doi.org/10.1109/TIA.2017.2686341.

[59] A. Jalilian, S. B. Naderi, M. Negnevitsky, M. T. Hagh, and K. M. Muttaqi, "Controllable DC-link fault current limiter augmentation with DC chopper to improve fault ride-through of DFIG," *IET Renewable Power Generation*, vol. 11, no. 2, pp. 313-324, 2017, https://doi.org/10.1049/iet-rpg.2016.0146.

[60] C. Nithya and J. P. Roselyn, "Development of grid-side converter-based FRT control and protection in a grid-connected solar photovoltaic park system under different control modes," *Frontiers in Energy Research*, vol. 10, 2022, https://doi.org/10.3389/fenrg.2022.1009196.

[61] H. Jia, H. Rao, C. Wen, and S. Mirjalili, "Crayfish optimization algorithm," *Artificial Intelligence Review*, vol. 56, pp. 1919–1979, 2023, https://doi.org/10.1007/s10462-023-10567-4.

[62] Y. Xiao, H. Cui, R. A. Khurma, A. G. Hussien, and P. A. Castillo, "MCOA: A Multistrategy Collaborative Enhanced Crayfish Optimization Algorithm for Engineering Design and UAV Path Planning," *International Journal of Intelligent Systems*, vol. 2025, no. 1, 2025, https://doi.org/10.1155/int/5054424.

[63] N. H. Shikoun, A. S. Al-Eraqi and I. S. Fathi, "BinCOA: An Efficient Binary Crayfish Optimization Algorithm for Feature Selection," *IEEE Access*, vol. 12, pp. 28621-28635, 2024, https://doi.org/10.1109/ACCESS.2024.3366495.

[64] B. Maiti *et al*., "Enhanced crayfish optimization algorithm with differential evolution's mutation and crossover strategies for global optimization and engineering applications," *Artificial Intelligence Review*, vol. 58, no. 3, p. 69, 2025, https://doi.org/10.1007/s10462-024-11069-7.

[65] S. Swain and P. K. Ray, "Short circuit fault analysis in a grid connected DFIG based wind energy system with active crowbar protection circuit for ridethrough capability and power quality improvement," *International Journal of Electrical Power & Energy Systems*, vol. 84, pp. 64-75, 2017, https://doi.org/10.1016/j.ijepes.2016.05.006.

[66] A. P. Schaffarczyk, "Introduction to Wind Turbine Aerodynamics," *Green Energy and Technology*, pp. 1–350, 2024, https://doi.org/10.1007/978-3-031-56924-1.

[67] G. Abad, J. Lopez, M. Rodriguez, L. Marroyo, and G. Iwanski, "Doubly fed induction machine: modeling and control for wind energy generation," *John Wiley & Sons*, vol. 85, 2011, https://doi.org/10.1002/9781118104965.

[68] M. N. Amin, M. A. Soliman, H. M. Hasanien, and A. Y. Abdelaziz, "Hybrid PSO-GSA algorithm-based optimal control strategy for performance enhancement of a grid-connected wind generator," *International*

Journal of Applied Power Engineering, vol. 10, no. 2, pp. 151-158, 2021, http://doi.org/10.11591/ijape.v10.i2.pp151-158.

[69] M. A. Soliman, H. M. Hasanien, H. Z. Azazi, E. E. El-kholy, and S. A. Mahmoud, "Hybrid ANFIS-GA-based control scheme for performance enhancement of a grid-connected wind generator," *IET Renewable Power Generation*, vol. 12, no. 7, pp. 832-843, 2018, https://doi.org/10.1049/iet-rpg.2017.0576.

[70] G. Rashid and M. H. Ali, "FRT Capability Enhancement of Offshore Wind Farm by DC Chopper," *Energies*, vol. 16, no. 5, p. 2129, 2023, https://doi.org/10.3390/en16052129.

[71] L. Xian, L. Wu, X. Zhang, and T. T. Pei, "Improving fault ride-through capability for doubly-fed induction generator based on improved system structure and corresponding control scheme," *IET Energy Systems Integration*, vol. 6, no. 1, pp. 73–85, 2024, https://doi.org/10.1049/esi2.12097.

[72] M. I. Mosaad, N. A. Sabiha, A. Abu-Siada and I. B. M. Taha, "Application of Superconductors to Suppress Ferroresonance Overvoltage in DFIG-WECS," *IEEE Transactions on Energy Conversion*, vol. 37, no. 2, pp. 766-777, 2022, https://doi.org/10.1109/TEC.2021.3126602.

[73] M. I. Mosaad, A. Abu-Siada, M. M. Ismaiel, H. Albalawi, and A. Fahmy, "Enhancing the fault ride-through capability of a DFIG-WECS using a high-temperature superconducting coil," *Energies*, vol. 14, no. 19, p. 6319, 2021, https://doi.org/10.3390/en14196319.

[74] S. B. Naderi, M. Negnevitsky and K. M. Muttaqi, "A Modified DC Chopper for Limiting the Fault Current and Controlling the DC-Link Voltage to Enhance Fault Ride-Through Capability of Doubly-Fed Induction-Generator-Based Wind Turbine," *IEEE Transactions on Industry Applications*, vol. 55, no. 2, pp. 2021-2032, 2019, https://doi.org/10.1109/TIA.2018.2877400.

[75] S. K. Tiwari, B. Singh and P. K. Goel, "Design and Control of Autonomous Wind–Solar System With DFIG Feeding 3-Phase 4-Wire Loads," *IEEE Transactions on Industry Applications*, vol. 54, no. 2, pp. 1119-1127, 2018, https://doi.org/10.1109/TIA.2017.2780168.

[76] A. Achar, Y. Djeriri, H. Benbouhenni, I. Colak, M. Oproescu, and N. Bizon, "Self-filtering based on the fault ride-through technique using a robust model predictive control for wind turbine rotor current," *Scientific Reports*, vol. 14, no. 1, 2024, https://doi.org/10.1038/s41598-023-51110-3.

[77] S. U. Islam and S. Kim, "Design and Implementation of Optimal Control Scheme for DFIG Based Wind Plant to Mitigate Sub-Synchronous Resonance Issues," *IEEE Access*, vol. 11, pp. 141162-141171, 2023, https://doi.org/10.1109/ACCESS.2023.3341884.

[78] M. N. Eskander and S. M. I. Amer, "Effect of the DC link Parameters on Transient Peaks and Harmonics Generated due to Grid Faults in Wind-Driven DFIG," *International Journal of Electrical Engineering and Computer Science*, vol. 7, pp. 8-16, 2025, https://doi.org/10.37394/232027.2025.7.2.

[79] P. Rajanala *et al*., "Intelligent MPPT and coordinated control for voltage stability in brushless DFIG wind turbines," *Scientific Reports*, vol. 15, no. 1, 2025, https://doi.org/10.1038/s41598-025-08676-x.

[80] A. A. Hossam-Eldin, E. Negm, M. S. Elgamal, and K. M. AboRas, "Operation of grid-connected DFIG using SPWM- and THIPWM-based diode-clamped multilevel inverters," *IET Generation, Transmission & Distribution*, vol. 14, no. 8, pp. 1412-1419, 2020, https://doi.org/10.1049/iet-gtd.2019.0248.

[81] A. Mirzakhani, R. Ghandehari, and S. A. Davari, "Performance improvement of DPC in DFIGs during unbalanced grid voltage based on extended power theory," *Ain Shams Engineering Journal*, vol. 12, no. 2, pp. 1775-1786, 2021, https://doi.org/10.1016/j.asej.2020.09.023.

[82] H. Chojaa *et al*., "Nonlinear Control Strategies for Enhancing the Performance of DFIG-Based WECS under a Real Wind Profile," *Energies*, vol. 15, no. 18, p. 6650, 2022, https://doi.org/10.3390/en15186650.